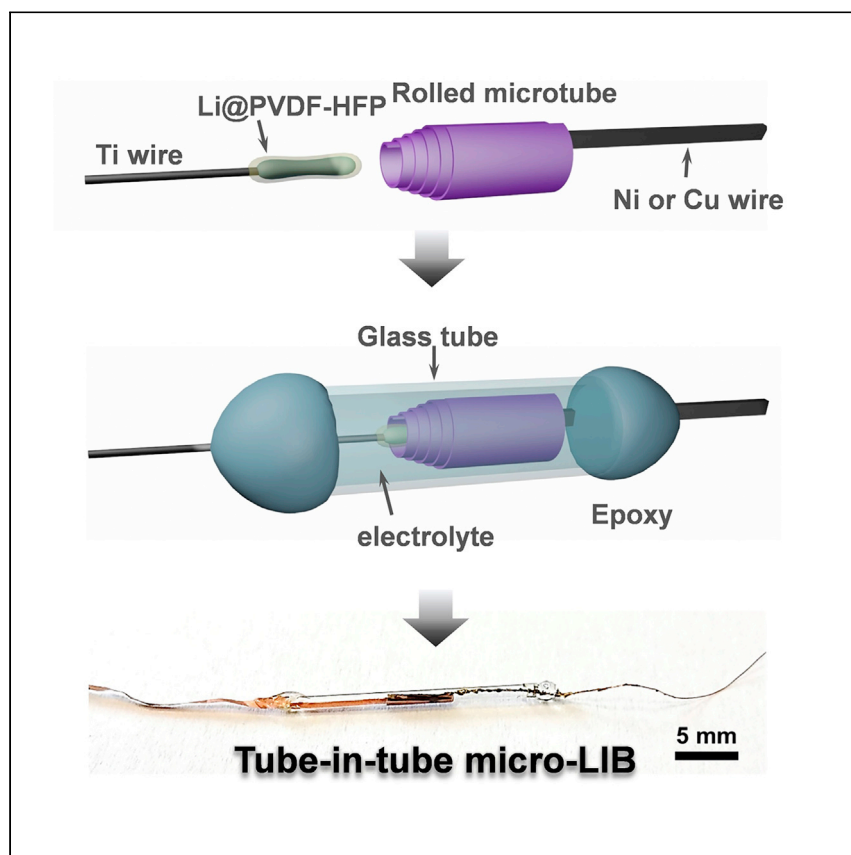


Report

A compact tube-in-tube microsized lithium-ion battery as an independent microelectric power supply unit



Miniaturized lithium-ion microbatteries as micropower sources often have considerable footprint areas and low areal energy densities and lack effective packaging technologies. Weng et al. propose a tube-in-tube configuration for microbatteries and achieve a small packaging footprint and high packaged areal energy density.

Qunhong Weng, Sitao Wang,
Lixiang Liu, ..., Yang Li, Felix
Gabler, Oliver G. Schmidt

wengqh@hnu.edu.cn

Highlights

A tube-in-tube conceptual configuration for microbatteries is proposed

The design tackles packaging and areal energy density problems

High packaged areal energy densities up to $605 \mu\text{Ah cm}^{-2}$ or $313 \mu\text{Wh cm}^{-2}$

The packaged micro-LIBs have small footprints of $0.39\text{--}0.79 \text{ mm}^2$

Weng et al., Cell Reports Physical Science 2, 100429

May 19, 2021 © 2021 The Authors.

<https://doi.org/10.1016/j.xcrp.2021.100429>



Report

A compact tube-in-tube micro-sized lithium-ion battery as an independent microelectric power supply unit

Qunhong Weng,^{1,2,4,*} Sitao Wang,¹ Lixiang Liu,¹ Xueyi Lu,¹ Minshen Zhu,¹ Yang Li,¹ Felix Gabler,^{1,3} and Oliver G. Schmidt^{1,3}

SUMMARY

Independent and well-packaged miniaturized energy storage devices (MESDs) are indispensable as power sources or backup units for integrated circuits and many dispersive electronics applications. Challenges associated with MESD development relate to their low packaged areal energy density and poor battery performance. Here, we propose a compact tube-in-tube battery configuration to overcome the areal energy density and packaging problems in microbatteries. Compact microtubular microelectrodes rolled up from patterned nanomembranes are sealed in an inert glass capillary with a thin tube wall. The resultant tube-in-tube micro-sized lithium-ion batteries (micro-LIBs), based on various active materials, exhibit very high and scalable packaged areal energy densities up to 605 microampere hours per square centimeter ($\mu\text{Ah cm}^{-2}$) or 313 $\mu\text{Wh cm}^{-2}$ with footprints as small as 0.39–0.79 mm^2 . This approach is a practical alternative for microbattery microelectrode, packaging, and configuration innovations.

INTRODUCTION

With the miniaturization of biomedical devices, sensors, and portable and integratable electronics, development of miniaturized energy storage devices (MESDs) that can power these electronics practically and efficiently is needed. Currently, lithium-ion batteries (LIBs) dominate the market of power supply devices for portable electronics because of their high energy density, output voltage, cycling stability, and lack of memory effects. Thus, micro-sized LIBs should be suitable MESDs to power integrated electronics and microelectromechanical systems (MEMSs). However, with miniaturization of LIBs for use as micropower sources, many challenging problems need to be solved, such as a low energy density for a given footprint area and lack of effective packaging technologies for the microdevices.^{1–6}

To overcome these problems, a substantial amount of effort has been made. The first critical issue for MESDs is their low areal energy density. Linear and planar configurations are common designs for MESDs.^{7–11} Although they can be small and provide many useful functions, such as flexibility and self-healing, the resultant low areal energy densities caused by low utilization of upper spaces in the chips are not well resolved. In recent years, 3D microelectrodes for MESDs on various substrates have received much attention, which could improve the areal energy and power density and solve this problem (G. Amatucci et al., 2006, ECS Meeting Abstracts, MA2005-02).¹² For example, Sun et al.¹³ reported fabrication of 3D micro-LIBs by 3D printing of $\text{Li}_4\text{Ti}_5\text{O}_{12}$ and LiFePO_4 as electrode materials. The

¹Institute for Integrative Nanosciences, Leibniz IFW Dresden, 01069 Dresden, Germany

²School of Materials Science and Engineering, Hunan University, Changsha 110016, China

³Materials, Architectures and Integration of Nanomembranes, Technische Universität Chemnitz, 09107 Chemnitz, Germany

⁴Lead contact

*Correspondence: wengqh@hnu.edu.cn
<https://doi.org/10.1016/j.xcrp.2021.100429>



micro-LIB has an unpackaged cell energy density of 2.6 milliwatt hours per square centimeter (mWh cm^{-2}) at a power density of 2.7 mW cm^{-2} . However, after packaging in a polymethyl methacrylate (PMMA) shell, the areal energy density was estimated to be only $\sim 35 \text{ } \mu\text{Wh cm}^{-2}$ with a device footprint area of $\sim 50 \text{ mm}^2$.¹³ Létiche et al.¹⁴ built a vertical silicon microtube array scaffold for micro-LIBs and boosted the areal capacity of a planar microbattery from $3.5 \text{ } \mu\text{Ah cm}^{-2}$ to 0.37 mAh cm^{-2} for a 3D micro-LIB without packaging. In addition, some micro-LIBs built from 3D interdigitated electrodes have also been proposed and tested without consideration of the packaging volume. Furthermore, using template-assisted electrodeposition on bi-continuous nanoporous electrodes, a fabricated 3D micro-LIB based on a Ni-Sn anode and a LiMnO_2 cathode achieved a remarkable energy density of $225 \text{ } \mu\text{Wh cm}^{-2}$ and power density of $345 \text{ } \mu\text{W cm}^{-2}$.¹⁵ The same active electrode materials deposited on 3D interdigitated 3D Ni current collectors, which were fabricated by combining 3D holographic lithography with conventional photolithography, reached energy densities of up to $65 \text{ } \mu\text{Wh cm}^{-2}$ and showed supercapacitor-like power performance.¹⁶ A very recent progress reported by Sun et al.¹⁷ achieved a very high areal capacity of 0.15 mAh cm^{-2} for a 3D $\text{Li-V}_2\text{O}_5$ microbattery prepared using a combination of imprint lithography, self-assembly, and electrodeposition techniques. However, the areal capacity dropped to only $\sim 18.8 \text{ } \mu\text{Ah cm}^{-2}$ after packaging with a UV-curable resin with a device footprint area of $\sim 96 \text{ mm}^2$.¹⁷ However, for 3D micro-LIBs, current packaging materials and technologies occupy too much volume and have large footprints, and the polymeric sealing materials are also unable to efficiently prevent oxygen and water vapor penetration.^{18,19} Importantly, these polymeric sealing materials are not inert enough to avoid interactions and dissolution in organic LIB electrolyte solutions to achieve stable battery performance. Thus, even after packaging, electrochemical tests for most of the reported 3D micro-LIBs were still performed in an inert gas atmosphere.

Rolling up thin membranes into 3D tubular structures is a powerful alternative strategy to create high-performance microelectrodes for micro-LIBs. This process exploits the different built-in strains in planar nanomembranes and rearranges them into 3D micro- and nanotubular architectures via a simple rolling process. Over the last two decades, many inorganic microtubes have been fabricated and studied successfully, such as TiO_2 , ZnO , Si_xN_y , and Pd/Fe/Pd .^{20–23} Many of these novel microtubes have been explored for LIB applications.^{24–28} LIBs fabricated from these rolled microtubes could achieve improved cycling stability because of release of strain in the nanomembranes and heterogeneous multilayer designs.

For these reasons, we propose a compact tube-in-tube configuration as a package solution to achieve high-performance micro-LIBs (Figure 1). The inner microtube is rolled up from a patterned and multilayered membrane by strain nanotechnology. Metallic lithium coated on Ti wire surfaces serves as the counter electrode and is further protected by a porous polyvinylidene fluoride-co-hexafluoropropylene (PVDF-HFP) layer. The electrolyte solution is brought inside and forms an isolated liquid column for immersion of the two microelectrodes. They are loaded into a glass capillary with a diameter of 1.0 mm or less, and the two ends are sealed with an epoxy resin. This design minimizes use of polymeric packaging materials and prevents direct contact of the organic electrolyte solution with the epoxy resin to boost the cycling stability of the battery. In this work, different microtubes, including SnO_x , SnS_2 , and Si-Ge, are fabricated and tested to verify the effectiveness of this solution. Importantly, by combining a compact microelectrode and small and inert glass capillaries as the packaging material, the proposed tube-in-

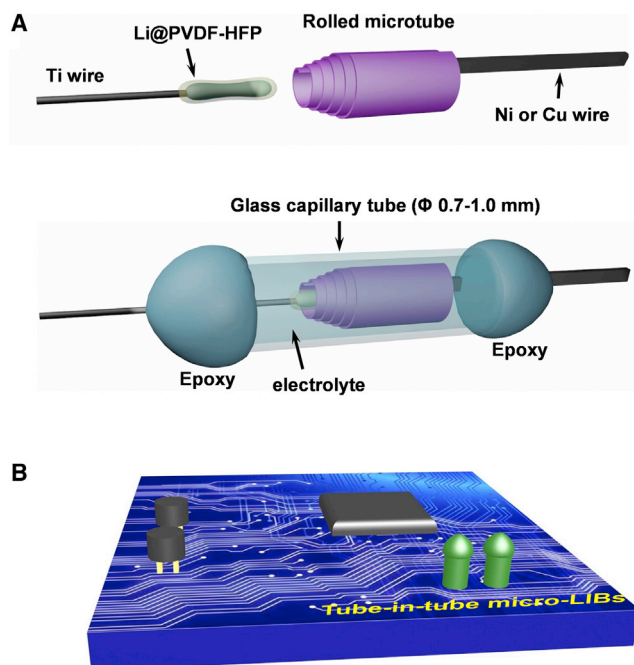


Figure 1. Conception of tube-in-tube micro-LIBs

(A) Schematic illustration of fabrication of a tube-in-tube micro-LIB. A single rolled microtube is pasted on a Ni or Cu wire, and the counter electrode comprises a metallic Li coating on a Ti wire along with a porous PVDF-HFP layer on the surface as a separator. After loading the microelectrodes into a glass capillary tube, a liquid electrolyte solution is added, and the two ends of the capillary tube are sealed by epoxy.

(B) Image illustrating use of tube-in-tube micro-LIBs as independent microelectronic units for integrated circuit power supply.

tube micro-LIBs achieve a high areal energy density and stable battery performance. The tube-in-tube micro-LIB is ready to be incorporated into an integrated circuit as an independent power supply component, similar to other microelectronic units.

RESULTS AND DISCUSSION

Rolling up nanomembranes

The microtubular electrode in the proposed tube-in-tube micro-LIB was fabricated using a rolling nanotechnology approach (Figures 2A and 2B). ARP3150 Photoresist was used as the sacrificial layer (SL), and the patterns were fabricated using photolithography. Then, the electrode layer (EL) and active material layer (AML) were deposited in sequence by e-beam evaporation with different thicknesses (Figure 2C). Different materials for the AML, including SnO_x , SnS_2 , Si-Ge and EL materials, such as Ni and Au, were investigated. As shown in Figures 2A and 2B, two main types of patterns were designed for fabrication of the microtubes: a square pattern (SP) with a size of 3.6 mm \times 3.6 mm and a long pattern (LP) with a length of up to 38.0 mm (3.0 mm \times 25.0 mm or 3.6 mm \times 38.0 mm). Different rolling lengths led to different numbers of rotations in the prepared microtubes and affected the resultant areal energy output for the assembled tube-in-tube micro-LIBs. We also introduced an array of microsized holes with a diameter of 60 μm on the multilayered membranes to shorten electrolyte ion transportation pathways in the final 3D microtubular electrode (Figure 2D). As shown in Figure 2E and Video S1, a fast rolling process was triggered after immersing the 3.0 mm \times 25.0 mm SnO_x/Ni LP substrate in acetone (etching solution), and the process of forming well-rolled and

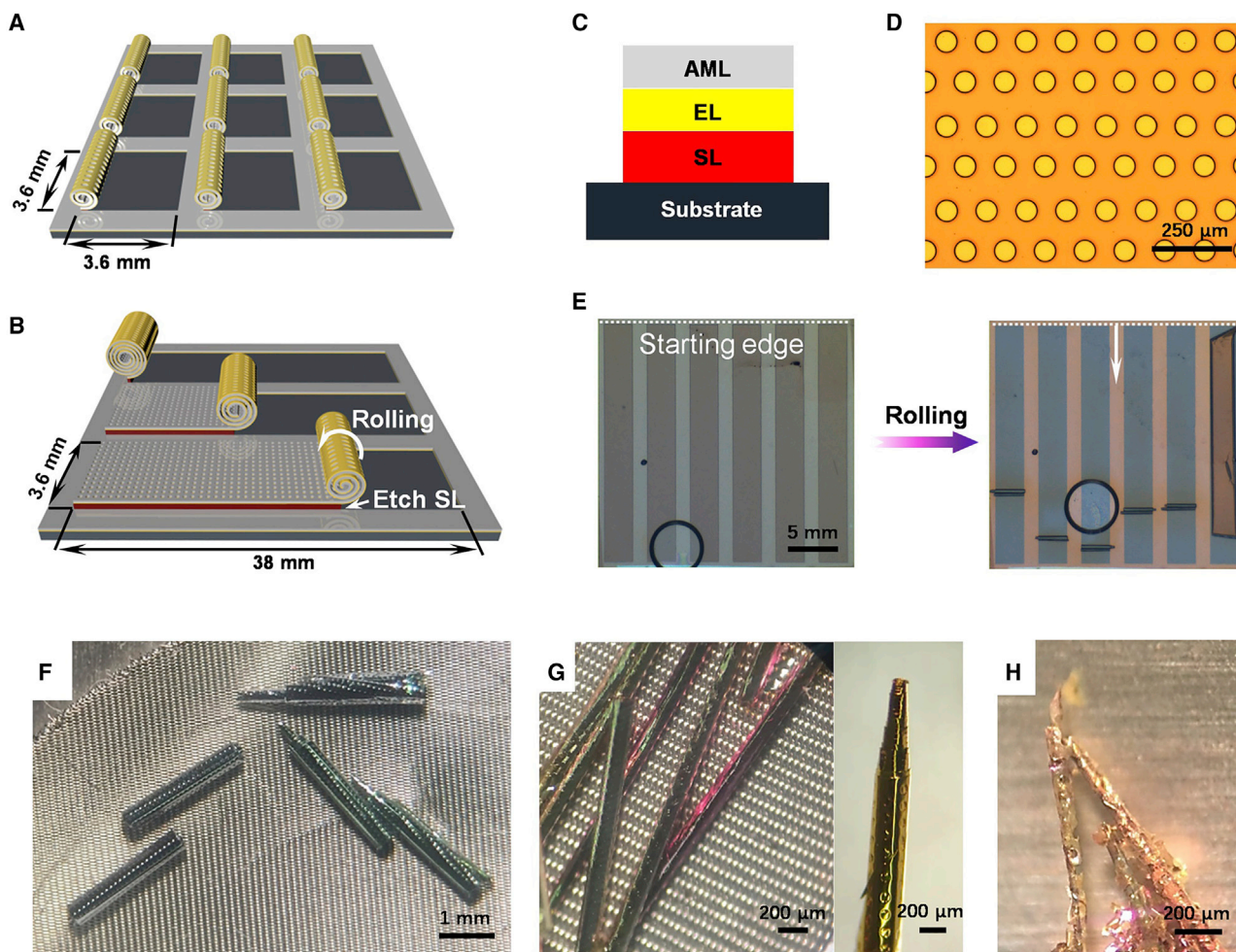


Figure 2. Design and fabrication of microtubes using a rolling nanotechnology approach using patterned multilayered membranes

(A and B) Schematics of rolling up multilayered membranes with a 3.6 mm × 3.6 mm square pattern (SP) and 3.6 mm × 38.0 mm long pattern (LP), respectively. The holes in the membranes were 60 μm in diameter and 125 μm in length.

(C) Illustration of the deposited multilayers. From top to bottom: activated material layer (AML; such as SnO_x, SnS₂, and Si/Ge), electrode layer (EL; such as Ni and Au), and sacrificial layer (SL; ARP3510 Photoresist).

(D) Optical image of the patterned SnO_x/Ni membrane.

(E) Optical images of the 3.0 mm × 25.0 mm SnO_x/Ni LP membrane before and after rolling. See also [Video S1](#). The circles in the images are air bubbles.

(F–H) Optical images of SnO_x/Ni microtubes rolled from the LP membrane (F), SnO_x/Au microtubes (G) obtained from the SP (left) and LP (right) membranes, and SnS₂/Au microtubes (H).

compact microtubes was finished in a few seconds. Simultaneous rolling from the opposite edge could be prevented completely after fixing them with a thin layer of protective polymer.

Accordingly, we prepared a series of microtubes for a tube-in-tube micro-LIB assembly, including SnO_x/Ni (thickness, 50 nm/25 nm), SnO_x/Au (50 nm/10 nm), SnS₂/Ti (50 nm/50 nm), SnS₂/Au (50 nm/10 nm), and Ge/Si/Au (20 nm/40 nm/20 nm); see [Figures 2F–2H](#), [S4](#), [S5](#), and [S8](#) for details. The resultant diameters for the obtained microtubes varied from ~100 to ~580 μm and were affected by the differential strain, which was deemed to be the driving force for rolling, and Young's modulus values and the thickness of the deposited membranes that could resist such a rolling process. The built-in differential strain of the membrane was dependent on the thermal expansion coefficient of the material, deposition rate, and other complex

factors, as discussed in previous work.²⁰ One should also take into consideration the thickness and Young's modulus of the membranes to reduce the resistance force for rolling. In our study, very different materials were deposited in sequence as the electrode functional layers to boost the differential strains in the membranes, whereas thin layers of the AML and EL were adopted to reduce the rolling resistance. The SnO_x/Ni microtube rolled from the LP membrane showed the largest diameter of ~580 μm, whereas the Ge/Si/Au microtubes had the smallest value of only ~100 μm. The number of rotations (n) could be calculated based on a formula for spiral length calculations: $n = 2L/\pi(D+d)$. Here, L is the rolling length, and D and d are the outer and inner diameters of the microtubes, respectively. The number of rotations for the LP-derived SnO_x/Au microtubes approached 70; the n values for the LP-derived SnO_x/Ni microtubes ranged from 20–32, and the SP-derived SnO_x/Au microtubes only had 5–10. These microtubes provided good samples to investigate the effect of the number of rotations on the areal energy output for tube-in-tube micro-LIBs.

Assembly of tube-in-tube micro-LIBs

Assembly of the tube-in-tube micro-LIBs was conducted under an optical microscope in a glovebox filled with Ar. A microtube fixed on a Cu or Ni wire was loaded carefully into a glass capillary under a microscope in a glove box. One end (2–3 mm) of a Ti wire was coated with molten metallic Li and additionally protected with a porous PVDF-HFP layer, and this structure was used as the counter electrode. Here the surface PVDF-HFP layer served as a separator between the cathode and anode as well as a protective layer for Li dendrite suppression.^{29,30} After loading the Li@PVDF-HFP electrode, the electrolyte solution (1 M LiPF₆) was in-taken by the capillarity to ensure that both microelectrodes were immersed in the liquid electrolyte solution. The two ends of the glass capillary were finally sealed with UV epoxy resin. LP- and SP-derived SnO_x/Au microtubes, SnS₂/Ti microtubes, and Ge/Si/Au microtubes were used for tube-in-tube micro-LIB assembly and tests.

For this tube-in-tube 3D design, the microelectrode was prepared by rolling a multi-layered thin membrane containing a metallic conducting layer and AMLs. After rolling, the microelectrode became a compact microtube with a small cross-section area, which not only made fabrication of high-areal-capacity micro-LIBs with small footprint areas possible but also provided well-designed 3D networks for electron transport. Such a design is helpful to boost the areal energy density and overcome the conduction problems of the 3D microelectrode to improve battery performance.

Evaluation of SnO_x tube-in-tube micro-LIBs

The chemical composition of the deposited SnO_x membrane from a SnO₂ target by e-beam evaporation is shown in Figure S2A; here, the x value was 1.1, which means that the compound was mainly composed of SnO with a minor amount of SnO₂. This was caused by partial loss of oxygen during electron beam heating and evaporation of the SnO₂ target. As shown in Figure 3A, the assembled SnO_x tube-in-tube micro-LIB had an outside diameter (O.D.) of 0.7 mm and a packaged footprint area of only 0.39 mm², which delivered a very stable open-circuit potential (OCP) of 3.2 V versus Li⁺/Li. The galvanostatic discharge/charge profiles in Figures 3B and S3 show two discharge plateaus at ~1.2 V and ~0.3 V, corresponding to the conversion reaction of SnO ($\text{SnO} + 2\text{Li}^+ + 2\text{e}^- \rightarrow \text{Li}_2\text{O} + \text{Sn}$) and alloying process of Sn ($\text{Sn} + x\text{Li}^+ + x\text{e}^- \rightarrow \text{Li}_x\text{Sn}$), respectively.^{31,32} Such reactions can be reversed well, as indicated by the charge profiles, which were stable during the repeated charge/discharge processes. The cyclic voltammetry (CV) of the SnO_x micro-LIB for the first 3 cycles at a scan rate

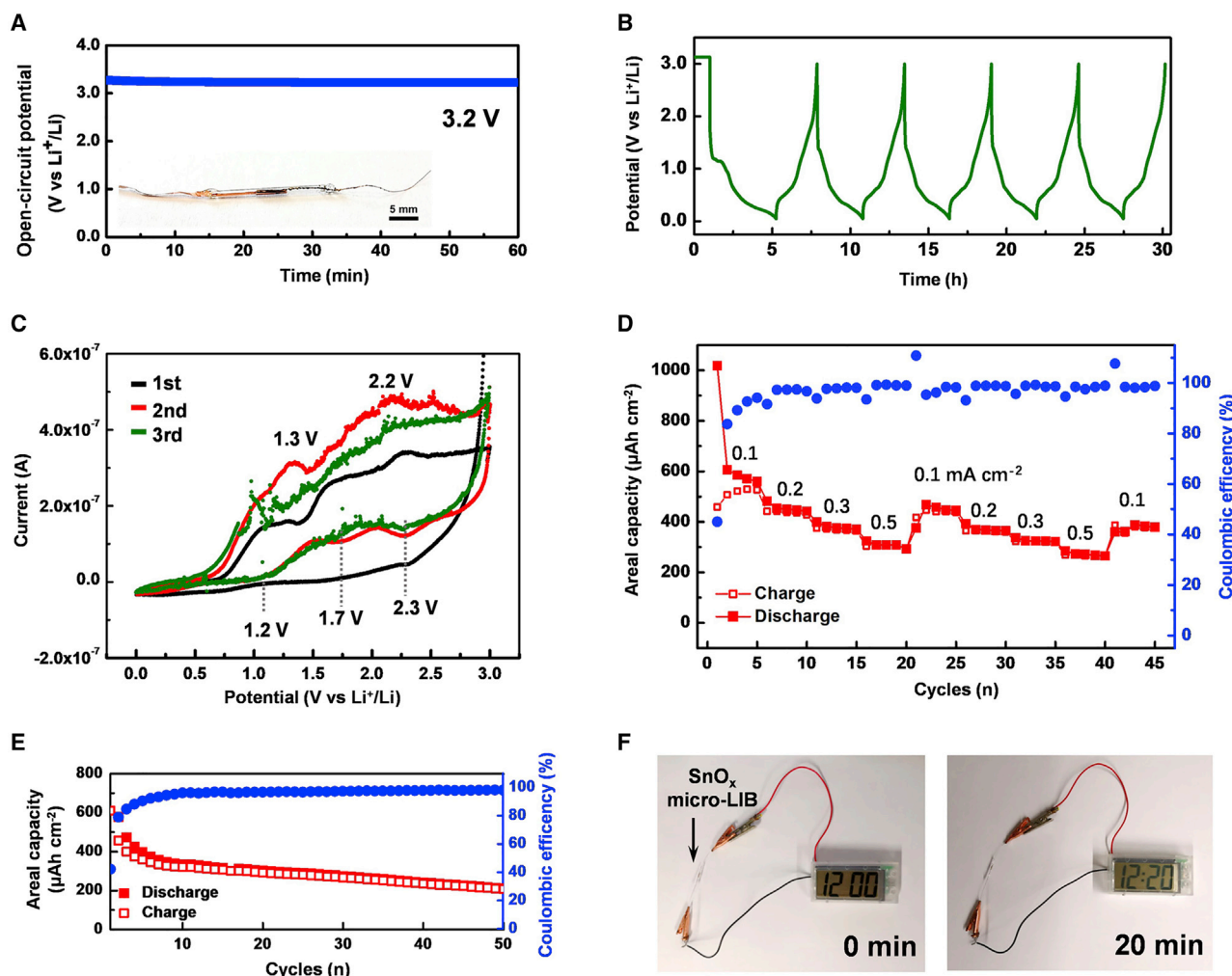


Figure 3. Electrochemical performances of tube-in-tube micro-LIBs based on SnO_x microtubes

- (A) OCPs of the assembled SnO_x micro-LIB. The inset shows a photograph of the assembled micro-LIB.
 (B) Galvanostatic discharge/charge profile of the micro-LIB at a current density of $200 \mu\text{A cm}^{-2}$, where the first hour was kept at an open-circuit status.
 (C) CV curves for the first 3 cycles at a scan rate of 0.1 mV s^{-1} .
 (D) Rate capability test and the corresponding Coulombic efficiencies.
 (E) Cycling stability and the corresponding Coulombic efficiency at a current density of $200 \mu\text{A cm}^{-2}$.
 (F) Photographs of the fabricated SnO_x tube-in-tube micro-LIB that powered a digital clock for over 20 min.

of 0.1 mV s^{-1} between 0.01 and 3.0 V is shown in Figure 3C. The broad cathodic peak at $\sim 1.2 \text{ V}$ and anodic peak at $\sim 1.3 \text{ V}$ were caused by reversible redox reactions between SnO and Sn . Redox peaks at higher potentials are a result of conversion between SnO and SnO_2 because of a minor amount of SnO_2 in SnO_x .³³

The SnO_x tube-in-tube micro-LIB exhibited an excellent rate capability, as shown in Figures 3D and S3. The packaged areal discharge and charge capacities at 0.1 mA cm^{-2} were 605 and $507 \mu\text{Ah cm}^{-2}$ (second cycle), respectively, and they were maintained at 324 and $303 \mu\text{Ah cm}^{-2}$ (16th cycle) when the current density increased to 0.5 mA cm^{-2} . The calculated packaged areal energy density was $313 \mu\text{Wh cm}^{-2}$ with a power density of $52 \mu\text{W cm}^{-2}$ during the second cycle, which is approximately one order of magnitude higher than that of a typical packaged 3D micro-LIB.^{13,17} The corresponding volumetric energy density was $157 \mu\text{Wh cm}^{-3}$ at $26 \mu\text{W cm}^{-3}$. When the current density

Table 1. Performance comparisons of the SnO_x tube-in-tube micro-LIBs rolled from different patterned membranes

Pattern type	Number of rotations	Reversible capacity at second cycle (μAh cm ⁻²)	Capacity retention (μAh cm ⁻²)	Coulombic efficiency (%)
LP	20–70	578 (discharge) 456 (charge)	216 (50 th)	42 (first) 79 (second) 98 (50 th)
SP	5–10	142 (discharge) 44 (charge)	38 (14 th)	23 (first) 31 (second) 72 (14 th)

was switched back to 0.1 mA cm⁻², the discharge and charge capacities recovered to 468 and 442 μAh cm⁻², respectively (22nd cycle). Such a good rate capability was also verified by a continued rate test. After 40 deep discharge/charge cycles at various rates, a high discharge capacity of 379 μAh cm⁻² was maintained in the 45th cycle, which was a retention of approximately 63% compared with that of the reversible capacity (second cycle) at the same rate with a Coulombic efficiency as high as 98.8%. The cycling stability of the SnO_x micro-LIB electrode was further proven by the galvanostatic discharge/charge cycling test results (Figure 3E), which are comparable with those from many bulk LIBs based on SnO active materials.^{31,32,34,35} The SnO or SnO₂ anode materials possess conversion and alloying/dealloying mechanisms in LIB applications, which undergo large volume changes during charge/discharge procedures.³⁶ Even with careful morphological or textural design, it is still difficult to completely overcome the quick capacity loss for this type of anode material.^{37–39} As a preliminary illustration of the power capability of the fabricated SnO_x tube-in-tube micro-LIB, we employed a single micro-LIB to power a digital clock and confirmed that the clock worked normally for at least 20 min (Figure 3F). This suggested the enormous potential of the tube-in-tube micro-LIBs for powering microelectronics and integrated circuits.

Effect of the nanomembrane pattern on battery performance

One of the main goals of MESD development is an areal capacity that is as high as possible. Thus, we also fabricated SnO_x tube-in-tube micro-LIBs with SP-derived microtubes for direct comparison. The performance of these microbatteries is summarized in Table 1. With an increase in rolling length from 3.6 mm (SP) to 38 mm (LP), the loaded active materials for the rolled 3D microtubes also increased by over 10 times. The reversible capacities can be improved by 4.1 times for the discharge and 10.4 times for the charge capacity. These results demonstrate the high scalability of the areal energy and power density for the developed tube-in-tube micro-LIBs. Furthermore, the LP microtube-based micro-LIB also exhibited a much better cycling stability and Coulombic efficiency (Figure S4). This suggests advantages for tube-in-tube designs that contain 3D microtubes rolled from ultralong patterns for development of compact and durable micro-LIBs.

Assembly and testing of SnS₂ and Si-Ge tube-in-tube micro-LIBs

In addition to SnO_x, we also assembled tube-in-tube micro-LIBs that were made from other rolled-up microtubes, such as SnS₂ and Si-Ge microtubes, to confirm the applicability of our proposed package solution for tackling micro-LIB challenges. We prepared SnS₂ microtubes through direct conversion of SnO_x microtubes by modified hydrothermal sulfurization.⁴⁰ After the reaction, the compact SnO_x membrane on the metallic substrate was converted into a SnS₂ layer composed of dense and vertically grown SnS₂ nanosheets (Figures S6 and S7). After assembly, the micro-LIB showed an OCP of 3.2 V (Figure S8) and relatively low areal energy densities (Figures S9 and S10). This was possibly caused by structural breakage of the microtubes

during hydrothermal sulfurization, as revealed by the optical and scanning electron microscopy (SEM) images (Figure S6).

For Si-Ge microtube micro-LIBs with an O.D. of 1.0 mm and packaged footprint area of 0.79 mm², the reversible cathodic peak at ~0.1 V and anodic peak at 0.5 V in the CV scans originated from lithiation and delithiation of Si and Ge, which are indistinguishable because of their close redox potentials (Figure S11A).^{25,30,41} The presence of Si in the microelectrode can be seen from the anodic peak at 0.2 V in the CV results, which was caused by delithiation of Li_xSi. The micro-LIB delivered a very high reversible areal discharge capacity of 840 μAh cm⁻² at a current density of 500 μA cm⁻² on the second cycle, which corresponds to a packaged areal energy density of 201 μWh cm⁻² with a power density of 120 μW cm⁻² or a volumetric energy density of 168 μWh cm⁻³ at 100 μW cm⁻³. Along with cycling, the capacity gradually decreased to 601 μAh cm⁻² (Figure S11B). At the same time, the Coulombic efficiency reached over 95%. Because Si and Ge are not stable LIB anode materials because of their large volume changes during alloying-dealloying electrochemical processes, the present cycling performances are comparable with bulk LIB performance using the same Si-Ge microtubes as the anode materials (Figure S12). These results further confirmed that our proposed packaging method for micro-LIBs is highly effective and comparable with other common sealing technologies for micro-LIBs, as summarized in Table S1.

Along with the abovementioned numerous advantages of the tube-in-tube solutions for micro-LIB research, there are problems that need to be addressed. The active materials in tubular electrodes are essentially nanometre-thick membranes that lack structural and textural engineering to optimize their stability. Currently, active membranes that can be rolled into microtubes and used for LIB applications are mostly prepared by e-beam evaporation or other physical evaporation methods, which limits the available active materials. To further improve the areal energy density of the microbatteries, high-voltage cathode materials, such as LiCoO₂ and LiFePO₄,⁵ should be introduced into the rolled membranes after overcoming their strain problems. The fraction of the active materials in the whole micro-LIB is still small for the present fabricated devices; further improvement of the rolling nanotechnology to increase the compactness of the rolled 3D tubular electrodes is also needed. An optimal electrode configuration should be rolled by the multi-layered membranes deposited with the functional layers of anode, separator, cathode, and conductor together, which should lead to better overall battery performance, particularly power performance, as expected. We may expect broad application of this solution if these problems can be solved in the near future.

In summary, we proposed a package solution based on a tube-in-tube configuration to provide a practical route for solving areal energy density and packaging problems for microbatteries. Through a rolling nanotechnology approach, advanced microelectrodes were fabricated that consider mass/energy compactness, electrical/ionic conductivity, and battery configuration. Our package solution, which uses submillimeter-sized glass capillaries as a shell, with the two ends sealed by an epoxy resin, prevents contamination of organic electrolyte solutions by unstable resins; the latter is currently the dominant microbattery packaging material being researched. We fabricated a series of tube-in-tube micro-LIBs with a packaged footprint area of only 0.39–0.79 mm², including SnO_x, SnS₂, and Si-Ge, and verified the effectiveness and wide applicability of the present solutions for microbatteries. As a result of the proposed tube-in-tube design, we not only achieved a packaged areal energy density up to 605 μAh cm⁻² or 313 μWh

cm^{-2} and high cycling stability for the fabricated micro-LIBs but also verified the performance scalability of the 3D tubular microelectrodes for compact microbattery designs. More compact micro-LIBs with integration of anode and cathode materials in the same rolled membrane are in development.

EXPERIMENTAL PROCEDURES

Resource availability

Lead contact

Further information and requests for resources should be directed to and will be fulfilled by the lead contact, Prof. Qunhong Weng (wengqh@hnu.edu.cn).

Materials availability

This study did not generate new unique reagents.

Data and code availability

All of the data associated with this study are included in the article and supplemental information. Additional information is available from the lead contact upon reasonable request.

Fabrication of rolled-up microtubes

Patterns were fabricated by photolithography using ARP 3510 Photoresist (Allresist) spin coated on a clean Si wafer. After development and baking, a metallic layer was deposited by e-beam evaporation (BOC Edward FL400, Germany) under a high vacuum at a pressure of less than 10^{-4} Pa. The deposition rate and thickness were monitored by a quartz crystal microbalance in the e-beam chamber. The adopted deposition rates for different materials were 1.0 \AA s^{-1} for Ni, Ge, Si, and SnO_x ; 1.5 \AA s^{-1} for Ti; and 0.5 \AA s^{-1} for Au. For the rolling up experiments, the substrate was immersed in acetone by one edge first, and then the patterned membranes were immersed continuously and slowly along with the rolling, or it was immersed completely in acetone after being placed into an axial magnetic field when Ni was used as the current collector (Figure S1).²³ Finally, the obtained microtubes were dried using a critical point dryer (CPD) to maintain the tubular structures.

Material characterization

The samples and rolled-up microtubes were characterized by Raman spectroscopy (Renishaw InVia, 442 nm), SEM (Zeiss, DSM982), and Auger electron spectroscopy (JEOL Jamp 9500 at a pressure of 10^{-7} Pa). We prepared a SnO_x membrane with a thickness of ~ 300 nm by e-beam deposition on a Ti film to perform Auger electron spectroscopy. Using a thick layer of the SnO_x ensured a high signal-to-noise ratio for the elemental analysis.

Assembly of tube-in-tube Li-ion microbatteries

Assembly of the micro-LIBs was performed in an Ar-filled glovebox ($\text{H}_2\text{O} < 0.1$ ppm, $\text{O}_2 < 0.1$ ppm, MBraun, Germany). A Ni or Cu wire was pasted on a single microtube surface with silver paste and used as an anode. The anodic microelectrodes were annealed at 200°C for 2 h before use. The counter electrode was prepared by melting a Li pellet with an electric soldering iron and coating the surfaces of a Ti wire end with a length of 2–3 mm. To avoid contact and an electrical short between the two electrodes, a porous polymeric layer of PVDF-HFP was also coated on the Li surfaces by dipping the electrode into a 5% PVDF-HFP/acetone solution that was dried naturally in a glovebox 3 times. The anode and cathode microelectrodes were inserted into the glass capillary under an optical microscope that was in the glovebox. LiPF_6 (1 M) in a 1:1:1 ethylene carbonate:diethyl carbonate:dimethyl carbonate

solution (Merck) containing 2.0 wt % vinylene carbonate (Aldrich) was used as the electrolyte solution. After filling the capillary with the electrolyte solution and immersing the microelectrodes, the two ends of the capillary were quickly sealed by UV curable resin under UV light irradiation. All assembled microbatteries were aged for 8 h before being subjected to electrochemical studies.

Electrochemical characterization

All microbatteries were evaluated by galvanostatic charge/discharge on an Arbin BT2000 system under diverse current densities at a voltage range of 0.05–3.0 V. OCP and CV were performed at different scan rates using a Multi Autolab/M101 electrochemical workstation. The section area of the glass capillary was adopted as the projection area on the substrate surface for the microbattery for areal capacity, energy density, and power density calculations.

SUPPLEMENTAL INFORMATION

Supplemental information can be found online at <https://doi.org/10.1016/j.xcrp.2021.100429>.

ACKNOWLEDGMENTS

We thank Dr. Jiawei Wang at IFW Dresden for Raman spectrum measurements as well as Ronny Engelhard, Barbara Eichler, Sandra Nestler, and Dr. Stefan Baunack at IFW Dresden for technical support during the experiments. Assistance with development of the magnetic setup from the Research Technology Department of IFW Dresden is greatly appreciated. Q.W. acknowledges a research fellowship conferred by the Alexander von Humboldt Foundation.

AUTHOR CONTRIBUTIONS

Q.W. conceived the research, performed the experiments, and wrote the manuscript. S.W. prepared the Si-Ge batteries and tested their performance. F.G. performed magnetic field-assisted nanomembrane rolling. L.L., X.L., M.Z., Y.L., and F.G. were involved in material preparation and characterization. O.G.S. supervised the project. All authors were involved in data analysis and discussions of the results.

DECLARATION OF INTERESTS

The authors declare no competing interests.

Received: February 23, 2021

Revised: March 31, 2021

Accepted: April 19, 2021

Published: May 11, 2021

REFERENCES

- Liu, L., Weng, Q., Lu, X., Sun, X., Zhang, L., and Schmidt, O.G. (2017). Advances on micro-sized on-chip lithium-ion batteries. *Small* 13, 1701847.
- Zhang, P., Wang, F., Yu, M., Zhuang, X., and Feng, X. (2018). Two-dimensional materials for miniaturized energy storage devices: from individual devices to smart integrated systems. *Chem. Soc. Rev.* 47, 7426–7451.
- Zheng, S., Shi, X., Das, P., Wu, Z.S., and Bao, X. (2019). The road towards planar microbatteries and micro-supercapacitors: from 2D to 3D device geometries. *Adv. Mater.* 31, e1900583.
- Jiang, K., and Weng, Q. (2020). Miniaturized energy storage devices based on two-dimensional materials. *ChemSusChem* 13, 1420–1446.
- Lai, W., Erdonmez, C.K., Marinis, T.F., Bjune, C.K., Dudney, N.J., Xu, F., Wartena, R., and Chiang, Y.-M. (2010). Ultrahigh-energy-density microbatteries enabled by new electrode architecture and micropackaging design. *Adv. Mater.* 22, E139–E144.
- Yue, X., Grzyb, J., Padmanabha, A., and Pikul, J.H. (2019). A minimal volume hermetic packaging design for high-energy-density micro-energy systems. *Energies* 13, 2492.
- Kwon, Y.H., Woo, S.W., Jung, H.R., Yu, H.K., Kim, K., Oh, B.H., Ahn, S., Lee, S.Y., Song, S.W., Cho, J., et al. (2012). Cable-type flexible lithium ion battery based on hollow multi-helix electrodes. *Adv. Mater.* 24, 5192–5197, 5145.
- Koo, M., Park, K.-I., Lee, S.H., Suh, M., Jeon, D.Y., Choi, J.W., Kang, K., and Lee, K.J. (2012). Bendable inorganic thin-film battery for fully

- flexible electronic systems. *Nano Lett.* **12**, 4810–4816.
9. Cras, F.L., Pecquenard, B., Dubois, V., Phan, V.P., and Guy-Bouyssou, D. (2015). All-solid-state lithium-ion microbatteries using silicon nanofilm anodes: high performance and memory effect. *Adv. Energy Mater.* **5**, 1501061.
 10. Wang, Y., Chen, C., Xie, H., Gao, T., Yao, Y., Pastel, G., Han, X., Li, Y., Zhao, J., Fu, K., et al. (2017). 3D-printed all-fiber Li-ion battery toward wearable energy storage. *Adv. Funct. Mater.* **27**, 1703140.
 11. Jiang, K., Zhou, Z., Wen, X., and Weng, Q. (2021). Fabrications of high-performance planar zinc-ion microbatteries by engraved soft templates. *Small* **17**, e2007389.
 12. Long, J.W., Dunn, B., Rolison, D.R., and White, H.S. (2004). Three-dimensional battery architectures. *Chem. Rev.* **104**, 4463–4492.
 13. Sun, K., Wei, T.S., Ahn, B.Y., Seo, J.Y., Dillon, S.J., and Lewis, J.A. (2013). 3D printing of interdigitated Li-ion microbattery architectures. *Adv. Mater.* **25**, 4539–4543.
 14. Létiche, M., Eustache, E., Freixas, J., Demortière, A., De Andrade, V., Morgenroth, L., Tilmant, P., Vaurette, F., Troadec, D., and Roussel, P. (2017). Atomic layer deposition of functional layers for on chip 3D Li-ion all solid state microbattery. *Adv. Energy Mater.* **7**, 1601402.
 15. Pikul, J.H., Gang Zhang, H., Cho, J., Braun, P.V., and King, W.P. (2013). High-power lithium ion microbatteries from interdigitated three-dimensional bicontinuous nanoporous electrodes. *Nat. Commun.* **4**, 1732.
 16. Ning, H., Pikul, J.H., Zhang, R., Li, X., Xu, S., Wang, J., Rogers, J.A., King, W.P., and Braun, P.V. (2015). Holographic patterning of high-performance on-chip 3D lithium-ion microbatteries. *Proc. Natl. Acad. Sci. USA* **112**, 6573–6578.
 17. Sun, P., Li, X., Shao, J., and Braun, P.V. (2021). High-performance packaged 3D lithium-ion microbatteries fabricated using imprint lithography. *Adv. Mater.* **33**, e2006229.
 18. Bjune, C.K., Marinis, T.F., and Chiang, Y.-M. (2015). Packaging design and assembly for ultrahigh energy density microbatteries. *J. Microelectron. Electron. Packag.* **12**, 129.
 19. Kyeremateng, N., and Hahn, R. (2018). Attainable energy density of microbatteries. *ACS Energy Lett.* **3**, 1172.
 20. Mei, Y., Huang, G., Solovev, A., Ureña, E., Mönch, I., Ding, F., Reindl, T., Fu, R., Chu, P., and Schmidt, O.G. (2008). Versatile approach for integrative and functionalized tubes by strain engineering of nanomembranes on polymers. *Adv. Mater.* **20**, 4085.
 21. Mei, Y., Solovev, A.A., Sanchez, S., and Schmidt, O.G. (2011). Rolled-up nanotech on polymers: from basic perception to self-propelled catalytic microengines. *Chem. Soc. Rev.* **40**, 2109–2119.
 22. Karnaushenko, D., Kang, T., Bandari, V.K., Zhu, F., and Schmidt, O.G. (2020). 3D self-assembled microelectronic devices: concepts, materials, applications. *Adv. Mater.* **32**, e1902994.
 23. Gabler, F., Karnaushenko, D.D., Karnaushenko, D., and Schmidt, O.G. (2019). Magnetic origami creates high performance micro devices. *Nat. Commun.* **10**, 3013.
 24. Ji, H.-X., Wu, X.L., Fan, L.Z., Krien, C., Fiering, I., Guo, Y.G., Mei, Y., and Schmidt, O.G. (2010). Self-wound composite nanomembranes as electrode materials for lithium ion batteries. *Adv. Mater.* **22**, 4591–4595.
 25. Yan, C., Xi, W., Si, W., Deng, J., and Schmidt, O.G. (2013). Highly conductive and strain-released hybrid multilayer Ge/Ti nanomembranes with enhanced lithium-ion-storage capability. *Adv. Mater.* **25**, 539–544.
 26. Wang, X., Chen, Y., Schmidt, O.G., and Yan, C. (2016). Engineered nanomembranes for smart energy storage devices. *Chem. Soc. Rev.* **45**, 1308–1330.
 27. Deng, J., Lu, X., Liu, L., Zhang, L., and Schmidt, O.G. (2016). Introducing rolled-up nanotechnology for advanced energy storage devices. *Adv. Energy Mater.* **6**, 1600797.
 28. Huang, S., Liu, L., Zheng, Y., Wang, Y., Kong, D., Zhang, Y., Shi, Y., Zhang, L., Schmidt, O.G., and Yang, H.Y. (2018). Efficient sodium storage in rolled-up amorphous Si nanomembranes. *Adv. Mater.* **30**, e1706637.
 29. Lu, Y., Tu, Z., and Archer, L.A. (2014). Stable lithium electrodeposition in liquid and nanoporous solid electrolytes. *Nat. Mater.* **13**, 961–969.
 30. Sun, X., Lu, X., Huang, S., Xi, L., Liu, L., Liu, B., Weng, Q., Zhang, L., and Schmidt, O.G. (2017). Reinforcing germanium electrode with polymer matrix decoration for long cycle life rechargeable lithium ion batteries. *ACS Appl. Mater. Interfaces* **9**, 38556–38566.
 31. Uchiyama, H., Hosono, E., Honma, I., Zhou, H., and Imai, H. (2008). A nanoscale meshed electrode of single-crystalline SnO for lithium-ion rechargeable batteries. *Electrochem. Commun.* **10**, 52.
 32. Ning, J., Jiang, T., Men, K., Dai, Q., Li, D., Wei, Y., Liu, B., Chen, G., Zou, B., and Zou, G. (2009). Syntheses, characterizations, and applications in lithium ion batteries of hierarchical SnO nanocrystals. *J. Phys. Chem. C* **113**, 14140.
 33. Wan, N., Lu, X., Wang, Y., Zhang, W., Bai, Y., Hu, Y.S., and Dai, S. (2016). Improved Li storage performance in SnO₂ nanocrystals by a synergetic doping. *Sci. Rep.* **6**, 18978.
 34. Ning, J., Dai, Q., Jiang, T., Men, K., Liu, D., Xiao, N., Li, C., Li, D., Liu, B., Zou, B., et al. (2009). Facile synthesis of tin oxide nanoflowers: a potential high-capacity lithium-ion-storage material. *Langmuir* **25**, 1818–1821.
 35. Iqbal, M.Z., Wang, F., Zhao, H., Rafique, M.Y., Wang, J., and Li, Q. (2012). Structural and electrochemical properties of SnO nanoflowers as an anode material for lithium ion batteries. *Scr. Mater.* **67**, 665.
 36. Wang, X., Weng, Q., Yang, Y., Bando, Y., and Golberg, D. (2016). Hybrid two-dimensional materials in rechargeable battery applications and their microscopic mechanisms. *Chem. Soc. Rev.* **45**, 4042–4073.
 37. Wang, X., Cao, X., Bourgeois, L., Guan, H., Chen, S., Zhong, Y., Tang, D., Li, H., Zhai, T., Li, L., et al. (2012). N-doped graphene-SnO₂ sandwich paper for high-performance lithium-ion batteries. *Adv. Funct. Mater.* **22**, 2682.
 38. Chen, J.S., and Lou, X.W. (2013). SnO₂-based nanomaterials: synthesis and application in lithium-ion batteries. *Small* **9**, 1877–1893.
 39. Zoller, F., Böhm, D., Bein, T., and Fattakhova-Rohlfing, D. (2019). Tin oxide based nanomaterials and their application as anodes in lithium-ion batteries and beyond. *ChemSusChem* **12**, 4140–4159.
 40. Zhai, C., Du, N., and Yang, H.Z.D. (2011). Large-scale synthesis of ultrathin hexagonal tin disulfide nanosheets with highly reversible lithium storage. *Chem. Commun. (Camb.)* **47**, 1270–1272.
 41. Yao, Y., McDowell, M.T., Ryu, I., Wu, H., Liu, N., Hu, L., Nix, W.D., and Cui, Y. (2011). Interconnected silicon hollow nanospheres for lithium-ion battery anodes with long cycle life. *Nano Lett.* **11**, 2949–2954.